Chapter 3

Hosotani's approach to the Schwinger model

In the 1990s, Yukio Hosotani *et al.* published several studies of the massive Schwinger model for an arbitrary number of $N > 1$ flavors at finite temperature T, where they reduced the massive model to a quantum mechanical system of $N - 1$ degrees of freedom [1–4]. This allowed them to derive analytic predictions for the boson masses that appear, and for the chiral condensate. In the massless N flavor model, it is known that a boson mass $\mu = \sqrt{Ng^2/\pi}$ appears [5]. In the Schwinger model with degenerate non-zero fermion mass the approach by Hosotani gives as a result N bosons, $N - 1$ of them with the same mass μ_2 and one with mass $\mu_1 > \mu_2$. In the limit $m \to 0$ one obtains $\mu_2 \to 0$ and $\mu_1 \to \mu$ [2, 4].

We will review the most important equations of this approach without complete derivations, together with a numerical solution for the predictions of the boson masses and the chiral condensate in the two flavor model at finite temperature. The reliability of these solutions is limited to $m \ll \mu$, as explained in Sections 6 and 8 of ref. [4].

3.1 Reduction to a quantum mechanical system

The QED Lagrangian for the N flavor Schwinger model in Euclidean space is given by

$$\mathcal{L} = \frac{1}{4} F_{\mu\nu} F_{\mu\nu} + \sum_{f=1}^{N} \overline{\psi}_f \left[\gamma_\mu^E \left(\partial_\mu + igA_\mu \right) + m_f \right] \psi_f. \tag{3.1}$$

The index f denotes the flavor. We consider degenerate fermion masses, that is $m_f \equiv m$. The idea is to map the model onto a circumference of length L_t and to impose the following boundary condition on the fermion fields and the gauge field

$$\begin{aligned} \psi_f \left(\tau + \frac{1}{T}, x \right) &= -e^{2\pi i \alpha_f} \psi_f(\tau, x), \\ A_\mu \left(\tau + \frac{1}{T}, x \right) &= A_\mu \left(\tau, x \right), \end{aligned} \tag{3.2}$$

where α_f is a phase factor and $T = 1/L_t$ denotes the temperature. By setting $\alpha_f = 0$ it is possible to relate the model on the circle with the finite temperature Schwinger model.

Next one uses the *bosonization method* to reduce the model to a quantum mechanical system of $N - 1$ degrees of freedom. The main idea is to write the fields in terms of bosonic operators that obey certain commutation relations, see e.g. refs. [3, 4]. However, those steps are rather tedious and here we only review the resulting formulation. After bosonization, the eigenvalue equation

$$\hat{H} \left| \Phi_0 \right\rangle = E_0 \left| \Phi_0 \right\rangle, \tag{3.3}$$

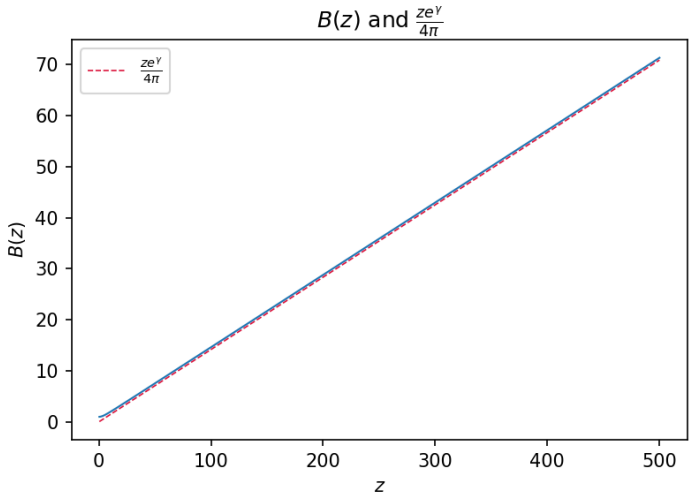

Figure 3.1: $B(z)$ defined in eq. (3.4). For large z, $B(z) \approx \frac{ze^\gamma}{4\pi}$.

where $\hat{H}$ is the Hamilton operator, $|\Phi_0\rangle$ is the vacuum state and E_0 its energy, is reduced to

$$
\begin{aligned}
&[-\triangle_\varphi + \kappa_0 F_N(\varphi_1, ..., \varphi_N)]\, g(\varphi_1, ..., \varphi_N) = \epsilon g(\varphi_1, ..., \varphi_N), \\
&\kappa_0 = \frac{N}{\pi(N-1)} m L_t \overline{B} e^{-\pi/(\mu N L_t)}, \quad F_N(\varphi_1, ..., \varphi_N) = -\sum_{f=1}^{N} \cos\varphi_f, \\
&\overline{B} = [B(\mu_1 L_t)]^{1/N} \, [B(\mu_2 L_t)]^{1-1/N}, \quad \epsilon = \frac{N L_t E_0}{2\pi} + \frac{\pi N^2}{12}, \\
&B(z) = \frac{z}{4\pi} \exp\left[\gamma + \frac{\pi}{z} - 2\int_1^\infty \frac{du}{(e^{uz}-1)\sqrt{u^2-1}}\right].
\end{aligned} \tag{3.4}
$$

$\gamma = 0.57721566490...$ is the Euler-Mascheroni constant. The angular variables φ_f are constrained by

$$
\varphi_N = \theta - \sum_{f=1}^{N-1} \varphi_f, \tag{3.5}
$$

where θ is the vacuum angle, which can be restricted to $(-\pi, \pi]$. It coincides with the vacuum angle that we introduced in Section 1.2 in a different form. $\triangle_\varphi$ is the Laplacian of the system, given by

$$
\begin{aligned}
\triangle_\varphi &= \sum_{f=1}^{N-1} \left(\frac{\partial}{\partial\varphi_f} - i\beta_f\right)^2 - \frac{2}{N-1} \sum_{f<f'}^{N-1} \left(\frac{\partial}{\partial\varphi_f} - i\beta_f\right)\left(\frac{\partial}{\partial\varphi_{f'}} - i\beta_{f'}\right) \\
\beta_f &= \alpha_f - \alpha_N.
\end{aligned} \tag{3.6}
$$

The function $B(z)$ has no direct physical meaning, but it appears in the equations. We show its behavior in figure 3.1. ϵ has to be determined together with $g(\varphi_1, ..., \varphi_N)$, μ_1 and μ_2 by solving the first line of eqs. (3.4) and other equations below. We are interested in a solution for μ_1 and μ_2.

The first line in eq. (3.4) is an eigenvalue problem for a system of $N-1$ degrees of freedom, due to the restriction (3.5). We simplify eqs. (3.4) for $N = 2$. The Laplacian is now given by

$$
\triangle_\varphi = \left(\frac{d}{d\varphi_1} + i\delta\alpha\right)^2 = -\left(i\frac{d}{d\varphi_1} - \delta\alpha\right)^2, \tag{3.7}
$$

with $\delta\alpha = \alpha_2 - \alpha_1$. In virtue of the constraint (3.5), the function $F_2(\varphi_1, \varphi_2)$ is expressed as

$$F_2(\varphi_1) = -\cos(\varphi_1) - \cos(\varphi_1 - \theta) = -2\cos\frac{\theta}{2}\cos\left(\varphi_1 - \frac{\theta}{2}\right). \tag{3.8}$$

Substituting $\triangle_\varphi$ and $F_2(\varphi_1)$ in the first line of eqs. (3.4) yields

$$\left[\left(i\frac{d}{d\varphi_1} - \delta\alpha\right)^2 - 2\kappa_0\cos\frac{\theta}{2}\cos\left(\varphi_1 - \frac{\theta}{2}\right)\right] g(\varphi_1) = \epsilon g(\varphi_1). \tag{3.9}$$

Let us define

$$\kappa \equiv 2\kappa_0\cos\frac{\theta}{2} = \frac{4}{\pi}mL_t\cos\frac{\theta}{2}\left[B(\mu_1 L_t)B(\mu_2 L_t)\right]^{1/2} e^{-\pi/(2\mu L_t)}, \tag{3.10}$$

thus, eq. (3.9) can be written as

$$\left[\left(i\frac{d}{d\varphi_1} - \delta\alpha\right)^2 - \kappa\cos\left(\varphi_1 - \frac{\theta}{2}\right)\right] g(\varphi_1) = \epsilon g(\varphi_1). \tag{3.11}$$

Finally, we substitute $\varphi = \varphi_1 - \frac{\theta}{2}$ and define $f(\varphi) = g(\varphi + \frac{\theta}{2})$. Then, eq. (3.11) takes the form

$$\left[\left(i\frac{d}{d\varphi} - \delta\alpha\right)^2 - \kappa\cos\varphi\right] f(\varphi) = \epsilon f(\varphi). \tag{3.12}$$

In refs. [1–4], it is shown that the masses μ_1, μ_2 and the chiral condensate $-\langle\overline{\psi}\psi\rangle_\theta$ can be obtained through the following equations, when $m \ll \mu$,

$$\begin{aligned}
\mu_2^2 &= \frac{2\pi^2}{L_t^2}\kappa\int_{-\pi}^{\pi} d\varphi\cos\varphi\,|f_0(\varphi)|^2, \\
\mu_1^2 &= \mu^2 + \mu_2^2, \\
\langle\overline{\psi}\psi\rangle_\theta &= -\frac{\mu_2^2}{4\pi m},
\end{aligned} \tag{3.13}$$

where $f_0(\varphi)$ denotes the ground state function of eq. (3.12), which obeys $f_0(\varphi+2\pi) = f_0(\varphi)$ and has to be normalized.

Now we need to find a solution to eq. (3.12) in order to calculate μ_2; however, κ also depends on μ_2. This means that eqs. (3.10), (3.12) and (3.13) must be solved in a self-consistent way. Analytically this is hardly possible for general values, but it can be done numerically. Still, there is one limiting case that is worth analyzing, because it will provide a cross-check with the numerical solutions of the next section. Let us set $\delta\alpha = 0$. We see in figure 3.1 that $B(z)$ is monotonically increasing, so if we restrict ourselves to the case $\cos(\theta/2) \geq 0$, for $\mu L_t \gg 1$ we have $\kappa \gg 1$. According to ref. [2], this allows us to approximate[1] $\cos\varphi \approx 1 - \frac{\varphi^2}{2}$ and eq. (3.12) reduces to

$$-\frac{d^2 f}{d\varphi^2} - \kappa\left(1 - \frac{\varphi^2}{2}\right) f = \epsilon f. \tag{3.14}$$

With the ansatz $f(\varphi) = e^{-b\varphi^2}$ we obtain

$$-\frac{d^2 f}{d\varphi^2} - \kappa\left(1 - \frac{\varphi^2}{2}\right) f = \left(2b - 4b^2\varphi^2 - \kappa + \kappa\frac{\varphi^2}{2}\right) e^{-b\varphi^2}, \tag{3.15}$$

[1] In Hosotani's work this approximation is not clearly argued, but it is necessary in order to obtain a limiting case that is already known in the literature, as we mention at the end of this section.

then

$$\epsilon = 2b - 4b^2\varphi^2 - \kappa + \kappa\frac{\varphi^2}{2}. \tag{3.16}$$

Let us remember that ϵ is a constant (see for instance the third line of eq. (3.4)), so it cannot depend on φ, which forces us to fix $b = \sqrt{\kappa/8}$. As a result, the normalized solution to eq. (3.12), under the previous assumptions, is

$$f(\varphi) = \frac{e^{-\sqrt{\frac{\kappa}{8}}\varphi^2}}{\int_{-\pi}^{\pi} d\varphi |e^{-\sqrt{\frac{\kappa}{8}}\varphi^2}|^2}. \tag{3.17}$$

To calculate μ_2 we denote

$$I \equiv \frac{\int_{-\pi}^{\pi} d\varphi \left(1 - \frac{\varphi^2}{2}\right) e^{-\sqrt{\frac{\kappa}{2}}\varphi^2}}{\int_{-\pi}^{\pi} d\varphi\, e^{-\sqrt{\frac{\kappa}{2}}\varphi^2}}, \tag{3.18}$$

in that manner we can rewrite the first line of eqs. (3.13) as

$$\mu_2^2 = \frac{2\pi^2}{L_t^2}\kappa I = \frac{8}{L_t^2\pi} m L_t \cos\frac{\theta}{2} \left[B(\mu_2 L_t) B(\mu_1 L_t)\right]^{1/2} e^{-\pi/(2\mu L_t)} I. \tag{3.19}$$

Since we consider $\mu L_t \gg 1$ then $e^{-\pi/(2\mu L_t)} \approx 1$. We are also able to obtain a simpler form of the function $B(z)$ in eq. (3.4). We see directly from its expression that if $z \gg 1$ the exponential term in the denominator of the integrand vanishes. Thus the integral is suppressed, together with the factor π/z. Then

$$B(z) \approx \frac{z e^{\gamma}}{4\pi}, \qquad z \gg 1, \tag{3.20}$$

see figure 3.1. With this result the value for μ_2 is approximately

$$\begin{aligned} \mu_2^2 &\approx \frac{8\pi^2}{L_t^2\pi} m L_t \cos\frac{\theta}{2} \left(\frac{\mu_1 L_t e^{\gamma}}{4\pi}\right)^{1/2} \left(\frac{\mu_2 L_t e^{\gamma}}{4\pi}\right)^{1/2} I \\ &= 2m \cos\frac{\theta}{2} e^{\gamma} \sqrt{\mu_1\mu_2}\, I. \end{aligned} \tag{3.21}$$

Equation (3.13) is valid when $m \ll \mu$. That way, we can approximate μ_1 by $\mu = \sqrt{2}g/\sqrt{\pi}$, since it is its value when the fermions are massless. Now, let us analyze the integral I in eq. (3.18)

$$I = 1 - \frac{\int_{-\pi}^{\pi} d\varphi\, \frac{\varphi^2}{2} e^{-\sqrt{\frac{\kappa}{2}}\varphi^2}}{\int_{-\pi}^{\pi} d\varphi\, e^{-\sqrt{\frac{\kappa}{2}}\varphi^2}}. \tag{3.22}$$

We can use the error function to express the denominator

$$\int_{-\pi}^{\pi} d\varphi\, e^{-a\varphi^2} = \sqrt{\frac{\pi}{a}}\mathrm{erf}(\sqrt{a}\pi), \quad \text{where } a = \sqrt{\frac{\kappa}{2}}, \quad \mathrm{erf}(x) = \frac{2}{\sqrt{\pi}}\int_0^x dt\, e^{-t^2}. \tag{3.23}$$

By using the following property (see ref. [6] for the error function properties)

$$\int dx\, \mathrm{erf}(\sqrt{a}x) = x\,\mathrm{erf}(\sqrt{a}x) + \frac{1}{\sqrt{\pi a}} e^{-ax^2} + \text{constant} \tag{3.24}$$

and integrating by parts, it is possible to show that

$$\int_0^{\pi} d\varphi\, \varphi^2 e^{-a\varphi^2} = \frac{\sqrt{\pi}}{4a^{3/2}}\,\mathrm{erf}(\sqrt{a}\pi) - \frac{\pi}{2a} e^{-a\pi^2}. \tag{3.25}$$

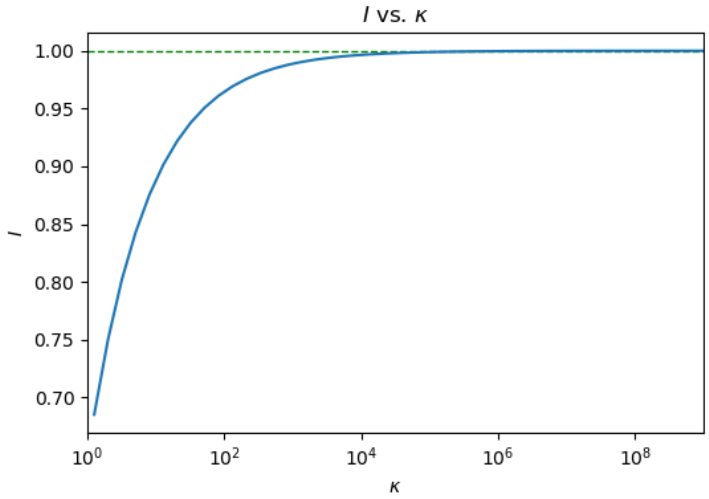

Figure 3.2: $I(\kappa)$ defined in eq. (3.22).

Therefore

$$\frac{\int_{-\pi}^{\pi} d\varphi \, \frac{\varphi^2}{2} e^{-\sqrt{\frac{\kappa}{2}}\varphi^2}}{\int_{-\pi}^{\pi} d\varphi \, e^{-\sqrt{\frac{\kappa}{2}}\varphi^2}} = \frac{1}{2a} - \frac{\sqrt{\frac{\pi}{a}} e^{-a\pi^2}}{\mathrm{erf}(\sqrt{a}\pi)}. \tag{3.26}$$

In the limit $L_t \to \infty$ we have $\kappa \to \infty$ and as a consequence $a \to \infty$. Thus, considering that

$$\lim_{a\to\infty} \mathrm{erf}(\sqrt{a}\pi) = 1, \tag{3.27}$$

we conclude

$$\lim_{L_t\to\infty} I = 1, \quad \text{when } \cos\frac{\theta}{2} \geq 0. \tag{3.28}$$

This can also be seen numerically, as shown in figure 3.2. Then, eq. (3.21) is simplified to

$$\mu_2^2 = 2e^{\gamma} m \sqrt{\mu\mu_2} \cos\frac{\theta}{2} \tag{3.29}$$

We are finally left with

$$\mu_2 = \left(4e^{2\gamma}\mu m^2 \cos^2\frac{\theta}{2}\right)^{1/3} = \left(4e^{2\gamma}\sqrt{\frac{2}{\pi}} g m^2 \cos^2\frac{\theta}{2}\right)^{1/3}. \tag{3.30}$$

We evaluate the constant terms

$$\left(4e^{2\gamma}\sqrt{\frac{2}{\pi}}\right)^{1/3} = 2.1633\ldots \tag{3.31}$$

Therefore

$$\mu_2 = 2.1633\ldots \left(m^2 g \cos^2\frac{\theta}{2}\right)^{1/3}, \quad L_t \to \infty, \quad \cos\frac{\theta}{2} \geq 0, \quad m \ll \mu. \tag{3.32}$$

The two flavor massive Schwinger model has a certain analogy to QCD, that way we can relate μ_1 with the mass of the η' meson and μ_2 with the pion mass (see Chapter 5). Anyhow, we will refer to the boson of mass μ_1 as η. So from now on we will denote $\mu_1 = m_\eta$ and $\mu_2 = m_\pi$. There are two predictions for m_π at infinite volume and small

fermion mass m. The first one is a semi-classical prediction [7], that is equal to eq. (3.32) by taking $\theta = 0$. The other prediction was deduced by A. Smilga [8] and it is slightly different from the semi-classical one: $m_\pi = 2.008(m^2 g)^{1/3}$.

It is possible to derive further expressions for limiting cases, however, the rest of the analysis will be done numerically.

3.2 Numerical solution

The first step to solve eqs. (3.10), (3.12) and (3.13) is to find a solution of the differential equation that involves $f(\varphi)$ with the condition $f(\varphi + 2\pi) = f(\varphi)$, $\varphi \in (-\pi, \pi]$. If one sets $\delta\alpha = 0$, performs the change of variable $\varphi = 2x$ and defines $a \equiv 4\epsilon$, $q \equiv -2\kappa$, then eq. (3.12) takes the form

$$\frac{d^2 f}{dx^2} + (a - 2q\cos 2x) f = 0, \quad f(x+\pi) = f(\pi), \quad x \in \left(-\frac{\pi}{2}, \frac{\pi}{2}\right], \tag{3.33}$$

which is the quantum pendulum equation [2] or the *Mathieu equation*. Furthermore, if $\delta\alpha \neq 0$ one can perform the change of variable $f(\varphi) = e^{-i\varphi\,\delta\alpha} g(\varphi)$. Thus, the derivatives and the boundary condition become

$$\begin{aligned} \frac{df}{d\varphi} &= e^{-i\delta\alpha}\left(\frac{dg}{d\varphi} - ig\,\delta\alpha\right), \\ \frac{d^2 f}{d\varphi^2} &= e^{-i\varphi\,\delta\alpha}\left(-2i\delta\alpha\frac{dg}{d\varphi} - \delta\alpha^2 + \frac{d^2 g}{d\varphi^2}\right), \\ g(\varphi + 2\pi) &= e^{i2\pi\delta\alpha} g(\varphi). \end{aligned} \tag{3.34}$$

Substituting in eq. (3.12) yields

$$-\frac{d^2 g}{d\varphi^2} - \kappa\cos\varphi\, g = \epsilon g. \tag{3.35}$$

This is the same equation for $f(\varphi)$ when $\delta\alpha = 0$ but with a different boundary condition given by the last line of eqs. (3.34)[2].

The solutions to eq. (3.33) are the *Mathieu functions* of first kind, denoted by

$$\frac{1}{\sqrt{\pi}}\mathrm{ce}_n\left(\frac{\varphi}{2}, -2\kappa\right), \quad \frac{1}{\sqrt{\pi}}\mathrm{se}_n\left(\frac{\varphi}{2}, -2\kappa\right), \quad n \text{ an even number}, \tag{3.36}$$

while the solutions to eq. (3.35) are non-periodic solutions to the Mathieu equation, known as *Floquet solutions*. There are some analytic expressions for the Mathieu functions ce_n, se_n, and the Floquet solutions. The former can be expressed as a linear combination of the sine and cosine functions, while the Floquet solutions are sought by using the so-called *Floquet theorem*, which allows us to find solutions of the form

$$F_\nu(\varphi) = e^{i\nu\varphi} P(\varphi). \tag{3.37}$$

Here ν is a constant, determined by the boundary condition, and $P(\varphi)$ is a periodic function. However, the result is quite complicated, see for example refs. [6, 10]. The best way to proceed is by discretizing eq. (3.12) in order to obtain a matrix eigenvalue problem that will allows us to find the ground state function $f_0(\varphi)$.

[2]For this reason, eq. (3.12) is also known as the *Damped Mathieu Equation*, see e.g. ref. [9].

Let us expand eq. (3.12)

$$-\frac{d^2f}{d\varphi^2} - 2i\delta\alpha\frac{df}{d\varphi} + \delta\alpha^2 f - \kappa\cos\varphi = \epsilon f \tag{3.38}$$

and divide the interval $(-\pi, \pi]$ in $N+1$ sites separated by $\Delta\varphi = 2\pi/N$. Then we replace the continuum derivatives by discrete derivatives

$$f_j = f(\varphi_j), \quad \frac{df}{d\varphi} \to \frac{f_{j+1} - f_{j-1}}{2\Delta\varphi}, \quad \frac{d^2f}{d\varphi^2} \to \frac{f_{j+1} - 2f_j + f_{j-1}}{\Delta\varphi^2},$$
$$\varphi \in (-\pi, \pi], \quad f_0 = f_N. \tag{3.39}$$

Substituting them in eq. (3.38) yields

$$-\frac{f_{j+1} - 2f_j + f_{j-1}}{\Delta\varphi^2} - 2i\delta\alpha\,\frac{f_{j+1} - f_{j-1}}{2\Delta\varphi} + \delta\alpha^2\, f_j - \kappa\cos\varphi_j\, f_j = \epsilon f_j. \tag{3.40}$$

The index j runs from 0 to $N-1$ (we are assuming $f_{-1} = f_{N-1}$ since f is periodic). Thus we have N algebraic equations that can be written in matrix form if we substitute

$$\frac{f_{j+1} - 2f_j + f_{j-1}}{\Delta\varphi^2} \quad \longrightarrow \quad \frac{1}{\Delta\varphi^2} \underbrace{\begin{pmatrix} -2 & 1 & 0 & 0 & \cdots & \cdots & \cdots & 1 \\ 1 & -2 & 1 & 0 & \cdots & \cdots & \cdots & 0 \\ 0 & 1 & -2 & 1 & \cdots & \cdots & \cdots & 0 \\ \vdots & \vdots & \vdots & \vdots & \cdots & 1 & -2 & 1 \\ 1 & 0 & 0 & 0 & \cdots & 0 & 1 & -2 \end{pmatrix}}_{\mathbb{M}_1} \underbrace{\begin{pmatrix} f_0 \\ f_1 \\ f_2 \\ \vdots \\ f_{N-1} \end{pmatrix}}_{\vec{f}},$$

$$\frac{f_{j+1} - f_{j-1}}{2\Delta\varphi} \quad \longrightarrow \quad \frac{1}{2\Delta\varphi} \underbrace{\begin{pmatrix} 0 & 1 & 0 & 0 & 0 & \cdots & 0 & -1 \\ -1 & 0 & 1 & 0 & 0 & \cdots & 0 & 0 \\ 0 & -1 & 0 & 1 & 0 & \cdots & 0 & 0 \\ 0 & 0 & -1 & 0 & 1 & \cdots & 0 & 0 \\ \vdots & \vdots & \vdots & \vdots & \vdots & \vdots & \vdots & \vdots \\ 0 & 0 & 0 & 0 & 0 & \cdots & 0 & 1 \\ 1 & 0 & 0 & 0 & 0 & \cdots & -1 & 0 \end{pmatrix}}_{\mathbb{M}_2} \begin{pmatrix} f_0 \\ f_1 \\ f_2 \\ \vdots \\ f_{N-1} \end{pmatrix},$$

$$\delta\alpha^2 f_j - \kappa\cos\varphi_j\, f_j \quad \longrightarrow \quad \underbrace{\mathrm{diag}(\delta\alpha^2 - \kappa\cos\varphi_0, \ldots, \delta\alpha^2 - \kappa\cos\varphi_{N-1})}_{\mathbb{M}_3}\vec{f}. \tag{3.41}$$

In that manner, the N algebraic equations can be expressed as

$$\left(-\frac{\mathbb{M}_1}{\Delta\varphi^2} - \frac{i\delta\alpha}{\Delta\varphi}\mathbb{M}_2 + \mathbb{M}_3\right)\vec{f} = \epsilon\vec{f}, \tag{3.42}$$

where $\mathbb{M}_1$, $\mathbb{M}_2$, $\mathbb{M}_3$ and $\vec{f}$ are defined in eq. (3.41). This is a linear algebra eigenvalue problem that can be solved using standard subroutines, e.g. LAPACK. Then, the eigenvectors $\vec{f}$ are obtained. However they are not yet normalized as $\int_{-\pi}^{\pi} d\varphi |f(\varphi)|^2 = 1$, so one must use a numerical integral (see Appendix B) to normalize the resultant vector $\vec{f}$.

Reference [2] mentions some limiting case solutions of the ground state of eq. (3.38)

$$f_0(\varphi) \approx \begin{cases} \frac{1}{\sqrt{2\pi}}\left[1+\frac{\kappa}{1-4\delta\alpha^2}(\cos\varphi - 2i\delta\alpha\sin\varphi)\right] & \text{for } \frac{\kappa}{1\pm 2\delta\alpha} \ll 1 \\ \frac{1}{\sqrt{2\pi}}\left[\frac{1}{\sqrt{2}}\left(1+e^{\mp i\varphi}\right)+\frac{\kappa}{4\sqrt{2}}\left(e^{\pm i\varphi}+e^{\mp 2i\varphi}\right)\right] & \text{for } \delta\alpha = \pm\frac{1}{2}, \quad \kappa \ll 1 \\ \frac{1}{\int_{-\pi}^{\pi}|e^{-i\delta\alpha\varphi-\sqrt{\frac{\kappa}{8}}\varphi^2}|^2 d\varphi} e^{-i\delta\alpha\varphi-\sqrt{\frac{\kappa}{8}}\varphi^2} & \text{for } \kappa \gg 1. \end{cases} \tag{3.43}$$

One can compare the numerical result with these particular expressions in order to verify the outcome of diagonalizing eq. (3.42). In figure 3.3 the comparison is shown.

The next step is to find solutions for m_π and the chiral condensate $\langle\overline{\psi}\psi\rangle = -m_\pi^2/(4\pi m)$. Equations (3.13) correspond to the following system of equations

$$\begin{aligned} \left[\left(i\frac{d}{d\varphi}-\delta\alpha\right)^2 - \kappa\cos\varphi\right] f(\varphi) &= \epsilon f(\varphi), \\ (m_\pi L_t)^2 &= 2\pi^2\kappa\int_{-\pi}^{\pi} d\varphi\, \cos\varphi\, |f_0(\varphi)|^2, \\ \kappa = \frac{4}{\pi} m L_t \cos\frac{\theta}{2}\, [B(m_\eta L_t)]^{1/2}\, [B(m_\pi L_t)]^{1/2}\, e^{-\pi/2\mu L_t}. & \end{aligned} \tag{3.44}$$

Below we are going to use the notation $\beta = 1/g^2$ and we recall that $\mu^2 = 2g^2/\pi$.

Equations (3.44) can be solved as a non-linear system of equations or in a self-consistent way. We explain both procedures as recipes. To solve eqs. (3.44) as a non-linear system one performs the following steps:

- First, one has to assign values to the input parameters κ, $\delta\alpha$, θ, β and m; that way one has to determine m_π and L_t.
- Then, the ground state function is calculated numerically by using eq. (3.42) for the κ and $\delta\alpha$ values that we chose, and the result is normalized.
- With f_0 already calculated, one computes $m_\pi L_t$ with the second equation of (3.44), using once again a numerical integrator.
- Note that $m_\pi L_t$ is already known from the previous step, but in order to find L_t and m_π separately one has to determine the "L_t-roots" of the last equation in (3.44). This can be done using a root finder, for instance bisection.

Following these four steps the system can be solved. It is important to note, however, that with this procedure one does not have control over L_t, but over κ, so if a solution for a specific L_t is desired, then a scan for several values of κ has to be applied. Still, it is possible to have control over L_t, but then one cannot give an initial value for m and it has to be determined in the same way we computed L_t in the last four steps. That is, one would have to do the following steps instead:

- Assign values to κ, $\delta\alpha$, θ, β, L_t and leave m_π and m undetermined.
- Calculate the normalized groundstate $f_0(\varphi)$.
- With f_0 already calculated, one computes m_π with the second equation of (3.44).
- Now one has to determine m in the last equation of (3.44). In this case one can solve for m analytically, there is no need for a root finder.

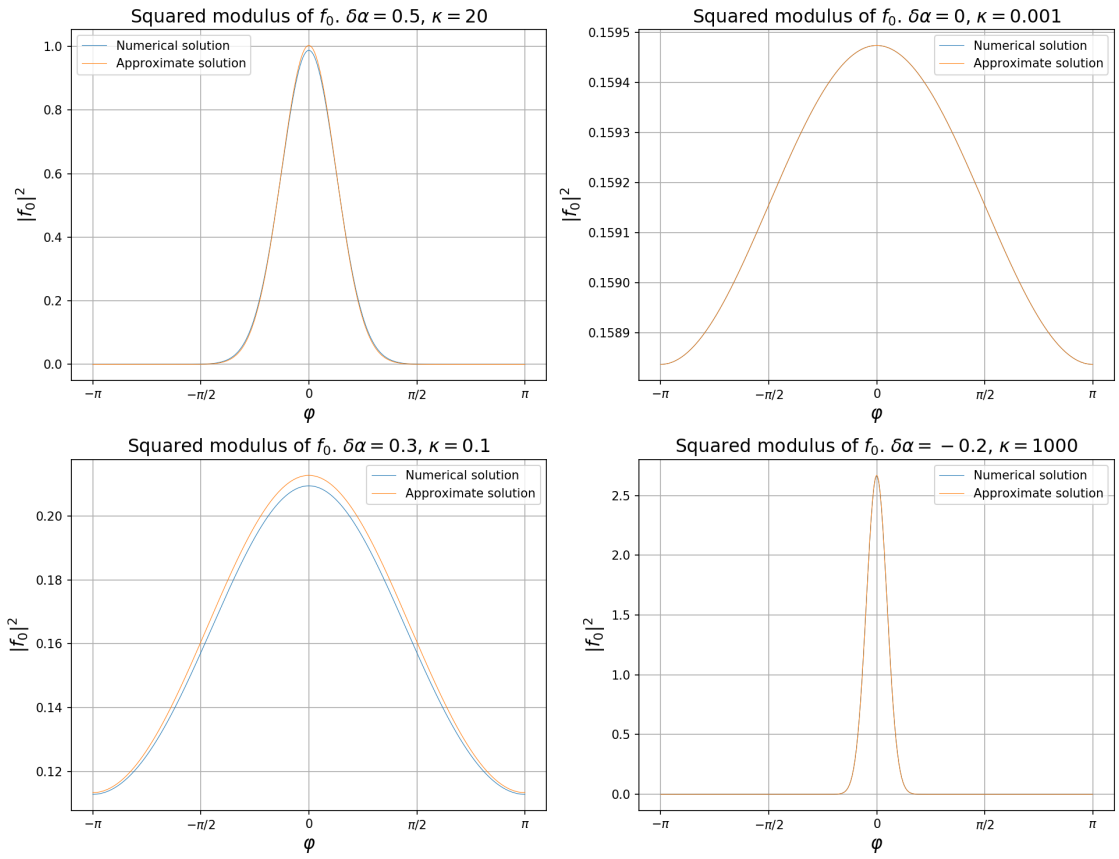

Figure 3.3: Ground state function of eq. (3.38). The approximate solutions correspond to the expressions in eq. (3.43). In the two plots on the right-hand side it is hard to distinguish the two curves. We use $N + 1 = 10^3$ points in the discretization.

On the other hand, if one wants to have total control over both variables, L_t and m, then the system has to be solved self-consistently. The idea is to carry out the following steps:

- Assign a value to $\delta\alpha$, θ, β, L_t, m and start from an initial guess for the pion mass m_π^{ini}. The pion mass will be determined self-consistently.
- Calculate κ.
- Calculate a new value of the pion mass, m_π^{new}, using the second equation of (3.44).
- If $|m_\pi^{\text{new}} - m_\pi^{\text{ini}}|$ is smaller than an error that one desires, then m_π^{new} is the result for m_π. Otherwise, one has to use m_π^{new} as m_π^{ini} and repeat these four steps until the final value has converged within the error. We cannot guarantee that the iteration converges, but in the examples that we tested the result always converges to the same values that one obtains with the two previous methods.

We implemented these three methods with Python and all of them give the same results. In general, the last one is most expensive computationally since one does not know how long the algorithm takes to converge and it depends on the initial guess. Anyhow, this method is most useful since we can fix arbitrary values of L_t and m. We choose these two parameters to be dimensionless, that way we set the energy scale of the system and compare the solution with the results of lattice simulations.

The first result to be revised is eq. (3.32), because it helps to verify the numerical solution and it also allows us to check the outcome with the three different methods

explained above. To do so, we substitute m_η for its value in the chiral limit ($m_\eta = \mu$) and then we solve eqs. (3.44). In figure 3.4 the pion mass is shown as a function of $(m^2 g)^{1/3}$ for different values of L_t and $\delta\alpha = \theta = 0$, $\beta = 4$. We see that when L_t becomes larger, the values move closer to the semi-classical prediction.

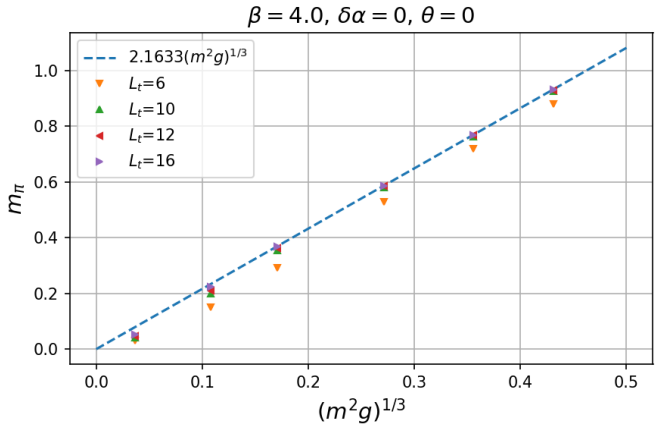

(a) Fixing m and determining L_t

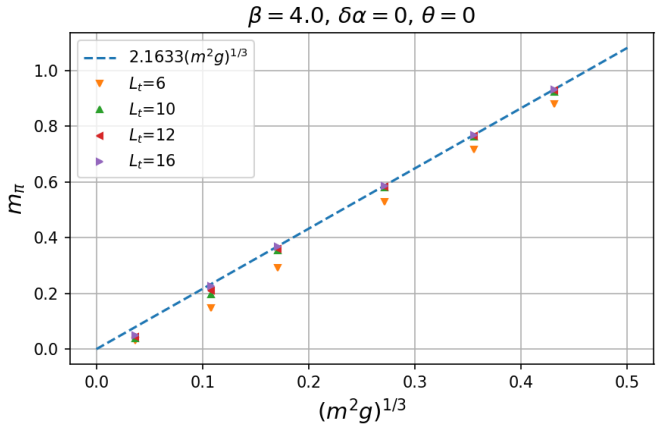

(b) Fixing L_t and determining m

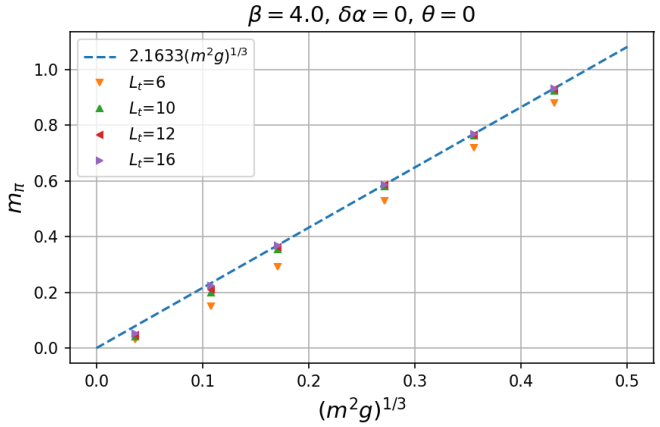

(c) Self-consistent solution

Figure 3.4: Solution for the pion mass as function of $(m^2 g)^{1/3}$ when one substitutes $m_\eta \approx \mu$. Each plot was made with one of the three different methods described above. We observe that the results coincide.

If one does not substitute $m_\eta \approx \mu$ and instead uses $m_\eta = \sqrt{m_\pi^2 + \mu^2}$, the result of figure 3.4 is different, since m_π will not converge to eq. (3.32). In figure 3.5, the pion mass as a function of $(m^2 g)^{1/3}$ and m_η as a function of m are shown, but taking into account the change in m_η. The chiral condensate can be calculated as well by using the third line of eqs. (3.13). Different values of this quantity as function of L_t and the temperature are shown in figure 3.6.

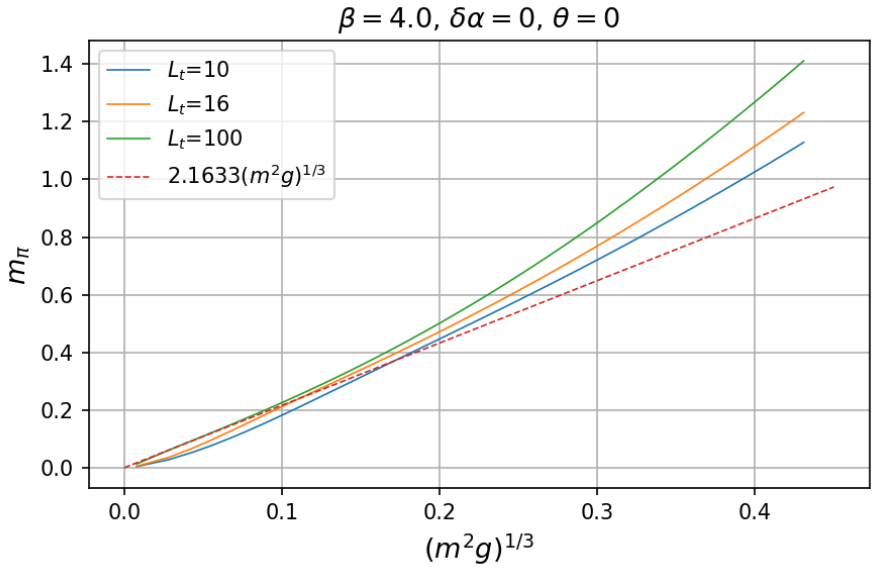

(a)

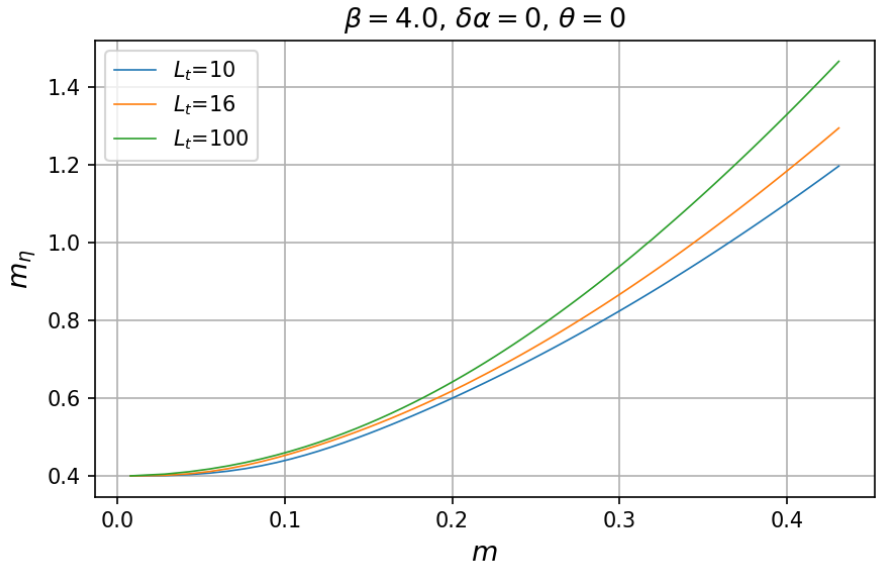

(b)

Figure 3.5: Predictions of m_η and m_π for different fermion masses and values of L_t. We see that as L_t becomes larger, for small m the value of m_π approaches to the semi-classical prediction and in the chiral limit it vanishes. We also observe that m_η converges to $\mu = \sqrt{2 \times 0.5^2/\pi} \simeq 0.39$ when $m \to 0$.

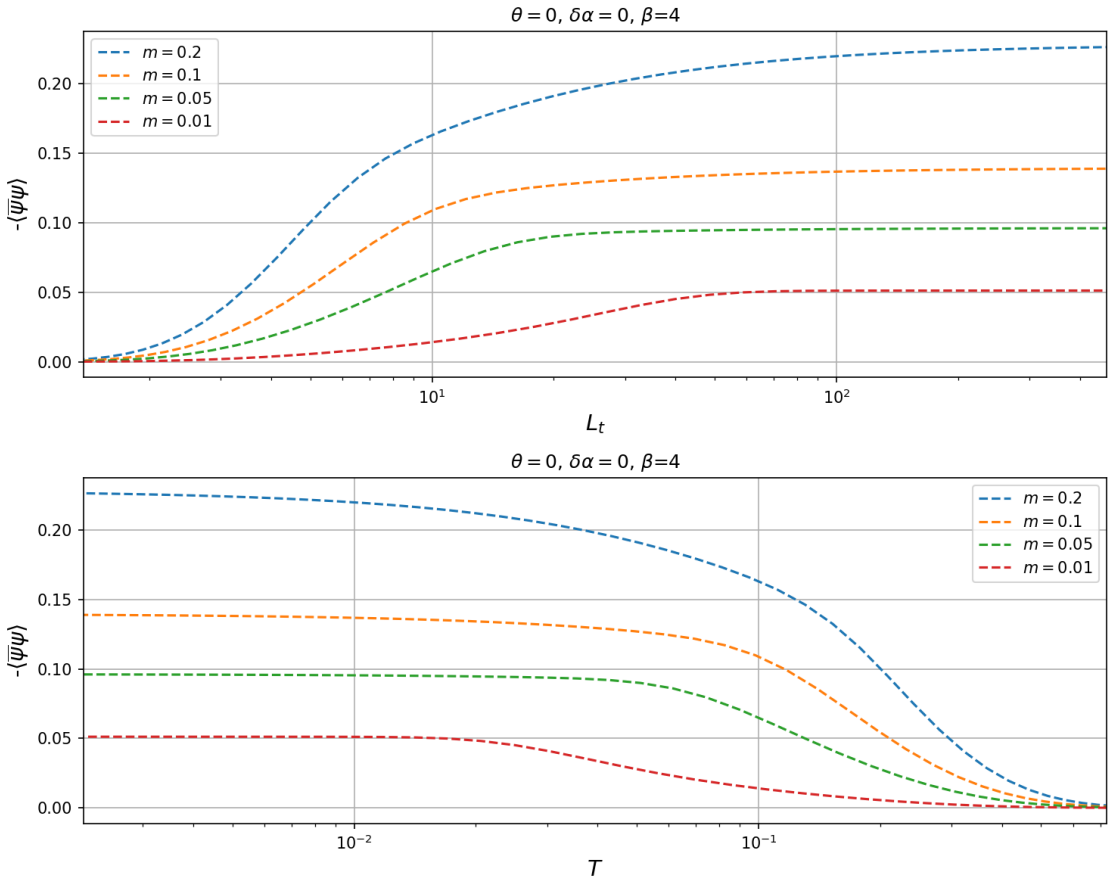

Figure 3.6: Predictions of the chiral condensate -$\langle\overline{\psi}\psi\rangle$ as a function of L_t and the temperature T. In the limit $m \to 0$, $\langle\overline{\psi}\psi\rangle$ vanishes. At high temperature the chiral condensate vanishes faster. We anticipated this result in Chapter 1, where we mentioned that only when we consider one flavor, $\langle\overline{\psi}\psi\rangle$ does not go to zero in the chiral limit.

3.3 Lattice simulations results

In this section we show results of m_π and m_η obtained with lattice simulations at finite temperature for $\beta = 1/g^2 = 4$. Each value of m_π and m_η was obtained through 10^3 measurements separated by 10 sweeps. 500 sweeps were performed to thermalize the configurations. The fermion mass was also measured, since it undergoes renormalization and one cannot use the bare Wilson fermion mass. We determined m by using the PCAC relation, see Section 4.4. We compare the results of the simulations with the prediction given by Hosotani, by setting $\delta\alpha = \theta = 0$. In figures 3.7, 3.8 and 3.9 results of m_π vs. $(m^2 g)^{1/3}$ and m_η vs. m for a spatial volume $L = 64$ and a time extent $L_t = 10, 12, 16$ are shown, respectively. These plots are in lattice units, *i.e.* we have set the lattice constant $a = 1$, so the masses do not have dimensions.

For $\beta = 4$, the mass of η in the chiral limit is $\sqrt{2 \times 0.5^2/\pi} \simeq 0.39$; then, one would expect Hosotani's prediction to match the simulation results for a fermion mass $m \ll 0.39$. This implies that the prediction should be valid when $(m^2 g)^{1/3} \ll 0.42$. In figure 3.7 we see that when $(m^2 g)^{1/3} \lesssim 0.1$, the analytic approach matches well the results of the simulations. For larger m, the values of m_π and m_η obtained by means of the simulations disagree with the prediction. Still, in both cases m_π is above the semi-classical prediction.

Now, if $(m^2 g)^{1/3} \lesssim 0.1$, then $m \lesssim 0.044$. According to figure 3.7 (b), in this region the prediction coincides with the simulation results. Both sets of results converge to a value

very close to 0.4, which is compatible with $m_\eta = \sqrt{2g^2/\pi}$. However, for masses larger than 0.05 we see again a discrepancy between the simulations and the analytic approach. In figures 3.8 and 3.9 we increase L_t and the agreement between the simulations and the prediction by Hosotani occurs when $m \lesssim 0.05$.

With the simulations we can also measure the chiral condensate. Even so, we cannot compare directly this result with the prediction by Hosotani, because, as we mentioned in Chapter 2, Wilson fermions break the chiral symmetry. Therefore, we do not see that $\langle\overline{\psi}\psi\rangle$ vanishes as m goes to zero. For instance, in figure 3.10 we show $\langle\overline{\psi}\psi\rangle$ for $L_t = 10$ and $L = 64$ as a function of the fermion mass.

Based on these results, we can affirm that the predictions of eqs. (3.44) do not allow us to perform a study for masses $m \gtrsim \sqrt{2g^2/\pi}$. Nevertheless, it is still useful to compare values near the chiral limit. The approach analyzed in this chapter for the Schwinger model at finite temperature would be more useful to compare results for the boson masses and the chiral condensate for arbitrary values of θ, close to $m = 0$. In principle, this is what Hosotani intended when he developed his solution. At finite θ, lattice simulations are not feasible due to the *sign problem*, where the action becomes complex and we cannot use $\exp(-S)$ as a probability weight factor. In this chapter we revised how far one can go with the outcome of eqs. (3.44) to study the finite temperature Schwinger model for arbitrary fermion mass.

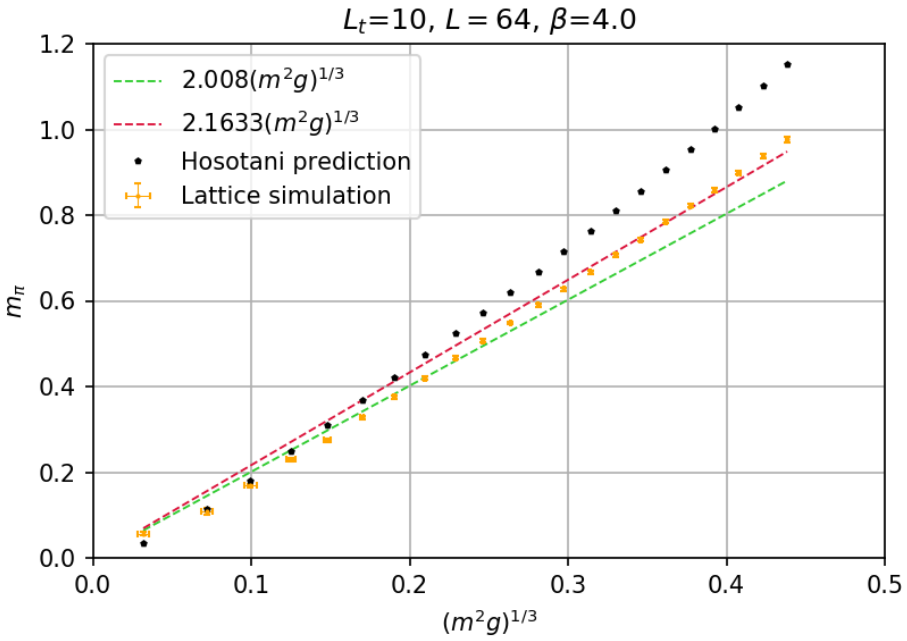

(a) m_π vs. $(m^2g)^{1/3}$

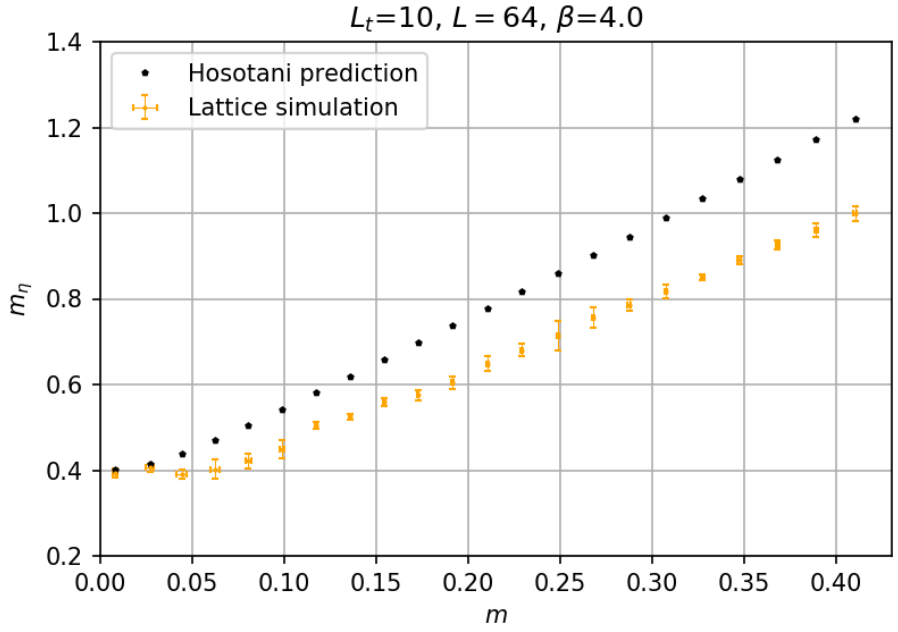

(b) m_η vs. m

Figure 3.7: Masses of the η and π mesons as a function of the degenerate fermion mass m for $L_t = 10$.

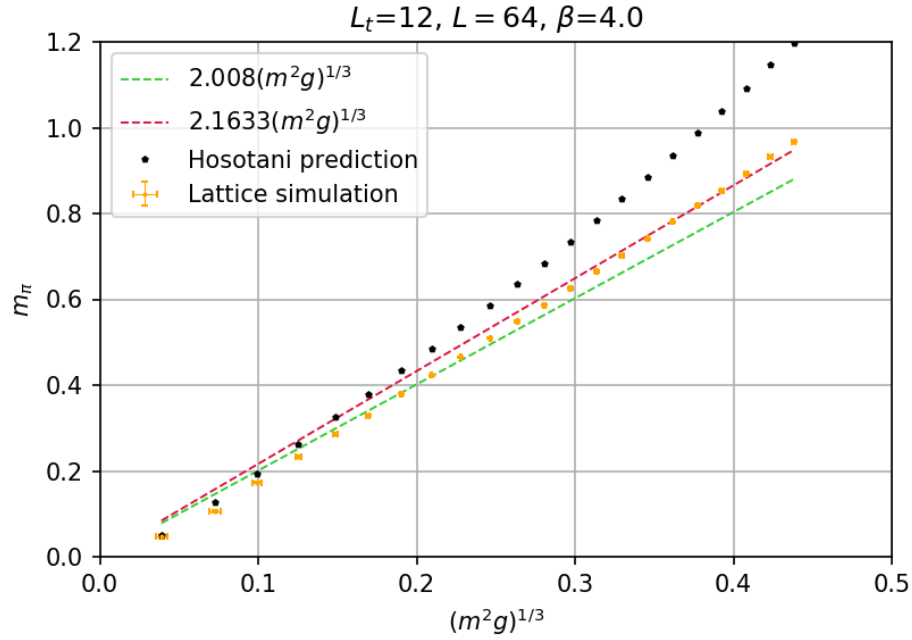

(a) m_π vs. $(m^2g)^{1/3}$

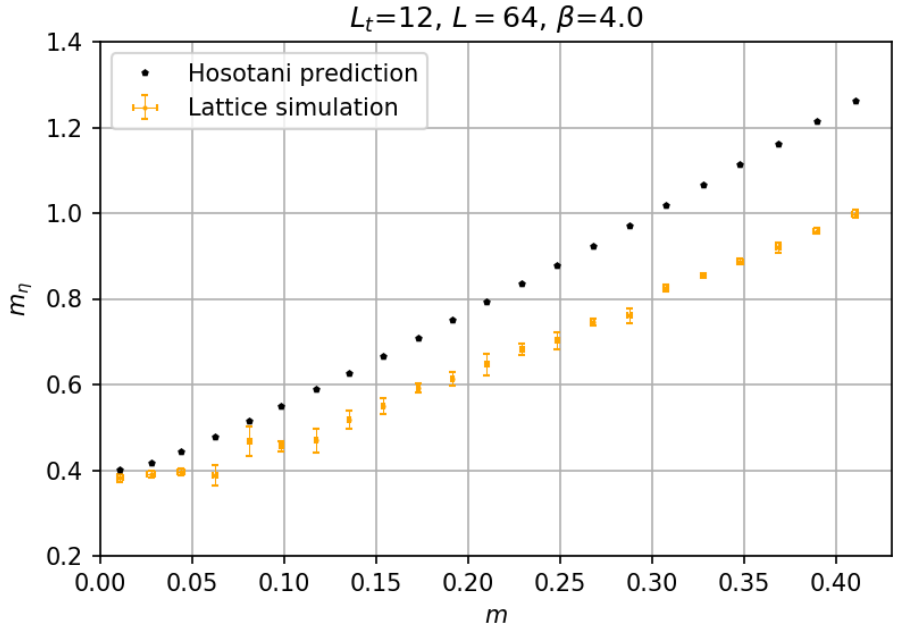

(b) m_η vs. m

Figure 3.8: Masses of the η and π mesons as a function of the degenerate fermion mass m for $L_t = 12$.

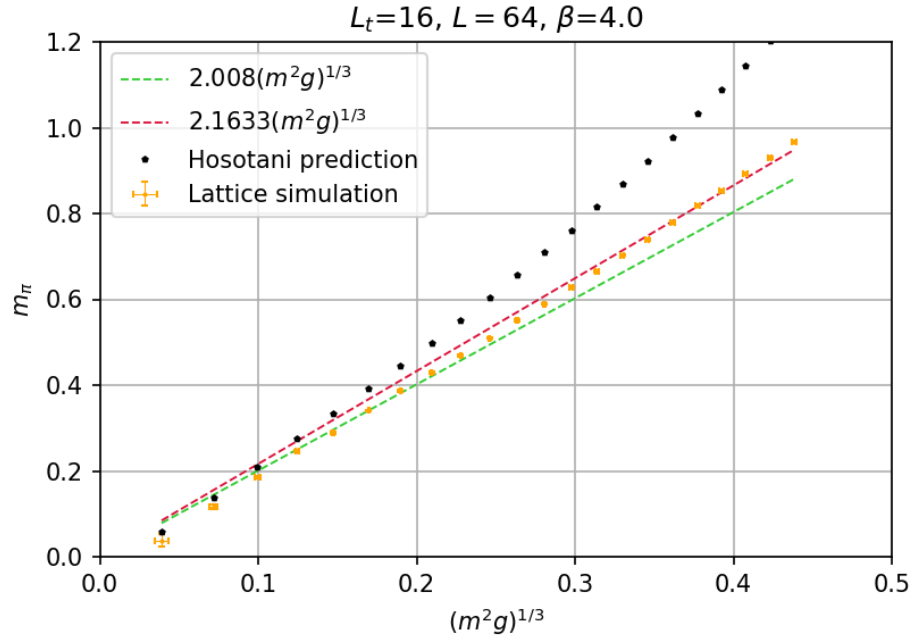

(a) m_π vs. $(m^2g)^{1/3}$

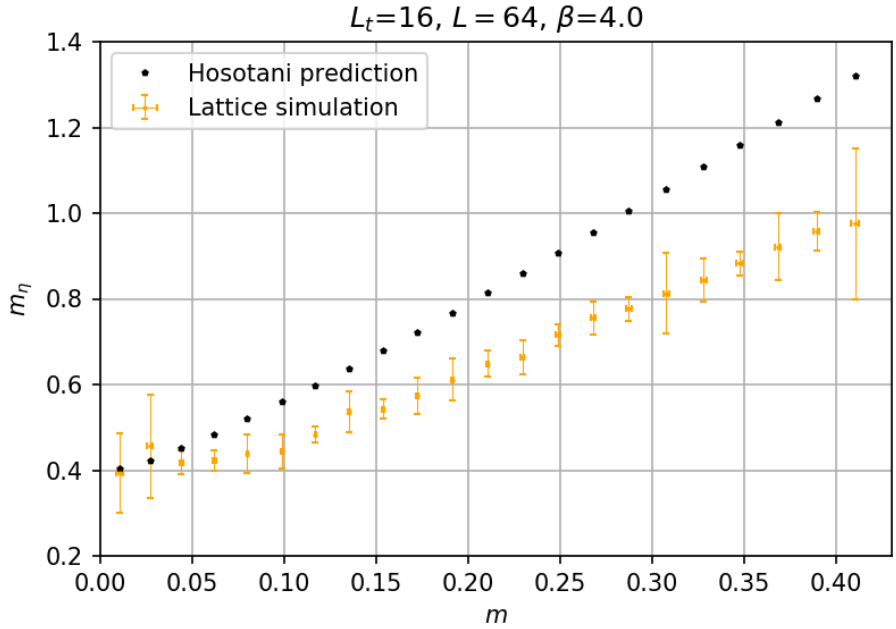

(b) m_η vs. m

Figure 3.9: Masses of the η and π mesons as a function of the degenerate fermion mass m for $L_t = 16$.

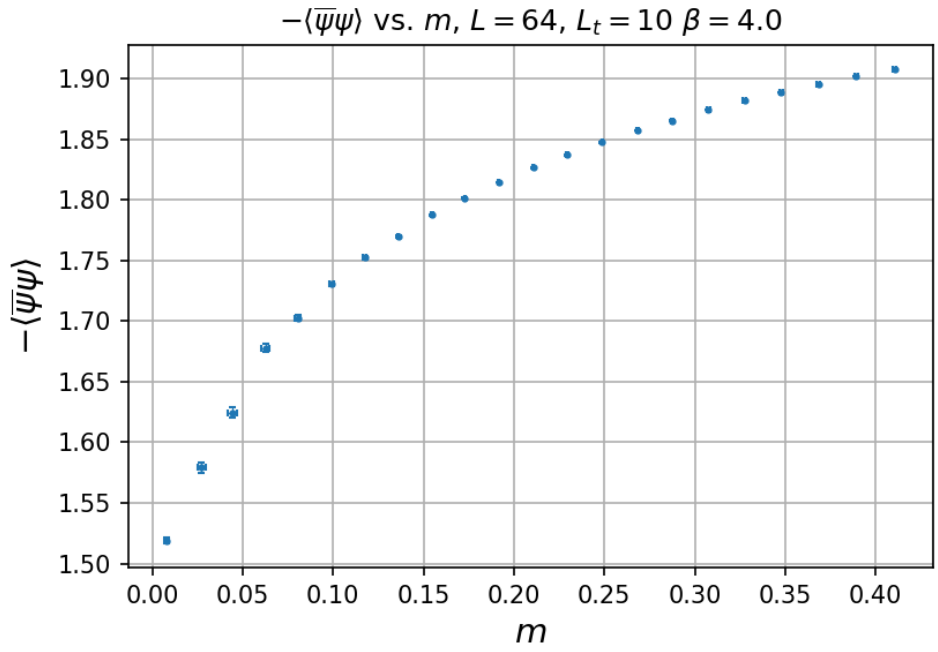

(a) $-\langle\overline{\psi}\psi\rangle$ vs. m obtained with lattice simulations.

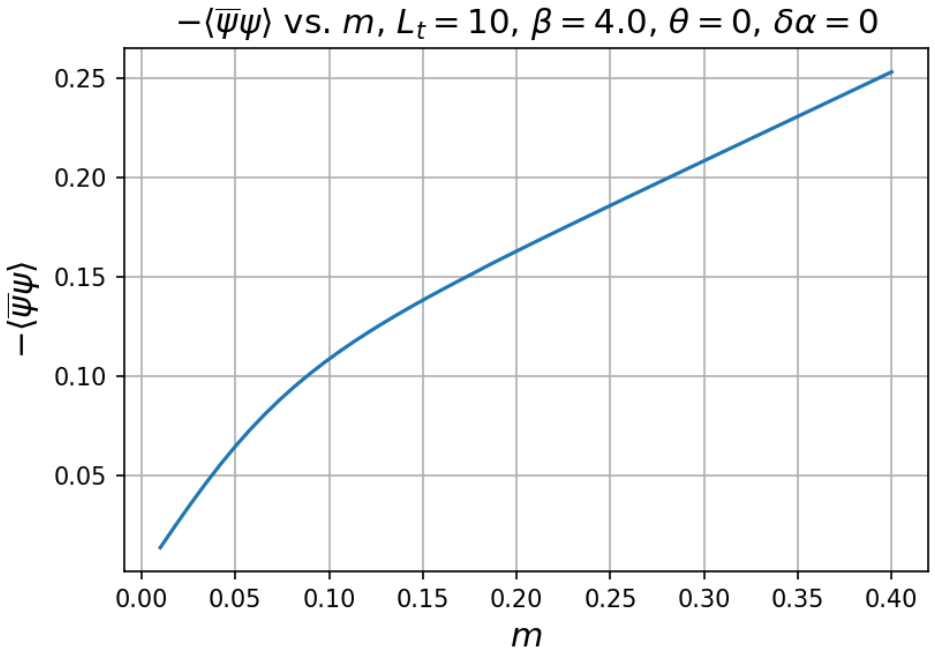

(b) $-\langle\overline{\psi}\psi\rangle$ vs. m obtained with eqs. (3.44) and the last line of eqs. (3.13).

Figure 3.10: In the upper plot, we show the result of $\langle\overline{\psi}\psi\rangle$ obtained with the lattice simulations, while in the lower plot we show the prediction by Hosotani. The former does not vanish in the chiral limit due to the explicit chiral symmetry breaking encoded in the Wilson fermion formulation.

Bibliography

[1] J.E. Hetrick, Y. Hosotani, and S. Iso. The massive multi-flavor Schwinger model. *Phys. Lett. B*, 350:92–102, 1995.

[2] Y. Hosotani. More about the massive multiflavor Schwinger model. In *Nihon University Workshop on Fundamental Problems in Particle Physics*, pages 64–69, 1995.

[3] J. E. Hetrick, Y. Hosotani, and S. Iso. Interplay between mass, volume, vacuum angle and chiral condensate in N flavor QED in two-dimensions. *Phys. Rev. D*, 53:7255–7259, 1996.

[4] Y. Hosotani and R. Rodriguez. Bosonized massive N-flavour Schwinger model. *J. Phys. A: Math. Gen*, 31:9925–9955, 1998.

[5] L. V. Belvedere, K. D. Rothe, B. Schroer, and J. A. Swieca. Generalized Two-dimensional Abelian Gauge Theories and Confinement. *Nucl. Phys. B*, 153:112–140, 1979.

[6] M. Abramowitz and I. A. Stegun. *Handbook of Mathematical Functions with Formulas, Graphs, and Mathematical Tables.* Dover, 1964.

[7] C. Gattringer, I. Hip, and C.B. Lang. The chiral limit of the two-flavor lattice Schwinger model with Wilson fermions. *Phys. Lett. B*, 466:287–292, 1999.

[8] A. V. Smilga. Critical amplitudes in two-dimensional theories. *Phys. Rev. D*, 55:R443–R447, 1997.

[9] D. Y. Hsieh. On Mathieu equation with damping. *J. Math. Phys.*, 21:722–725, 1980.

[10] N. W. McLachlan. *Theory and application of Mathieu functions.* Clarendon Press, Oxford, 1951.